Acta Pharmaceutica Sinica B 2021;11(4):1003−1009

Chinese Pharmaceutical Association
Institute of Materia Medica, Chinese Academy of Medical Sciences

Acta Pharmaceutica Sinica B

www.elsevier.com/locate/apsb
www.sciencedirect.com

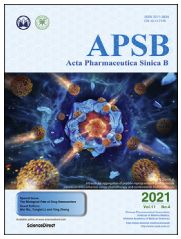

ORIGINAL ARTICLE

The biological fate of the polymer nanocarrier material monomethoxy poly(ethylene glycol)-*block*-poly(D,L-lactic acid) in rat

Xiangjun Meng[a,c], Zhi Zhang[a], Jin Tong[a], Hui Sun[a], John Paul Fawcett[a], Jingkai Gu[a,b,*]

[a]*Research Center for Drug Metabolism, School of Life Sciences, Jilin University, Changchun 130012, China*
[b]*Beijing Institute of Drug Metabolism, Beijing 102209, China*
[c]*School of Pharmaceutical Sciences, Tsinghua University, Beijing 100084, China*

Received 1 November 2020; received in revised form 23 December 2020; accepted 30 January 2021

KEY WORDS

Monomethoxy poly(ethylene glycol)-*block*-poly(D,L-lactic acid);
Polymer;
Nanocarrier material;
Pharmacokinetics;
Biodistribution;
Metabolism;
Excretion;
Rat

Abstract Monomethoxy poly(ethylene glycol)-*block*-poly(D,L-lactic acid) (PEG-PLA) is a typical amphiphilic di-block copolymer widely used as a nanoparticle carrier (nanocarrier) in drug delivery. Understanding the *in vivo* fate of PEG-PLA is required to evaluate its overall safety and promote the development of PEG-PLA-based nanocarrier drug delivery systems. However, acquiring such understanding is limited by the lack of a suitable analytical method for the bioassay of PEG-PLA. In this study, the pharmacokinetics, biodistribution, metabolism and excretion of PEG-PLA were investigated in rat after intravenous administration. The results show that unchanged PEG-PLA is mainly distributed to spleen, liver, and kidney before being eliminated in urine over 48 h mainly (>80%) in the form of its PEG metabolite. Our study provides a clear and comprehensive picture of the *in vivo* fate of PEG-PLA which we anticipate will facilitate the scientific design and safety evaluation of PEG-PLA-based nanocarrier drug delivery systems and thereby enhance their clinical development.

*Corresponding author.
E-mail address: gujk@jlu.edu.cn (Jingkai Gu).

Peer review under responsibility of Chinese Pharmaceutical Association and Institute of Materia Medica, Chinese Academy of Medical Sciences.

https://doi.org/10.1016/j.apsb.2021.02.018

1. Introduction

With continuous progress in the design and synthesis of polymer nanocarrier materials (PNMs)[1,2], a variety of nanomedicines based on PNMs have been approved by the U.S. Food and Drug Administration (FDA) for clinical trials[3–5]. This reflects the fact that PNMs have been generally considered to be non-toxic inert vehicles. However, emerging evidence has demonstrated that PNMs can not only change the pharmacokinetics of the loaded drug[6–14] but also introduce additional toxic effects by interacting with the body's immune system[15], metabolism and transport processes[16–18]. For example, PEGylated polymer materials such as 1,2-distearoyl-*sn*-glycero-3-phosphoethanolamine-polyethylene glycol) (DSPE-PEG) and monomethoxy poly(ethylene glycol)-*block*-poly(D,L-lactic acid) (PEG-PLA) which have good biocompatibility can cause IgM-based immune responses[19]. Polymers such as surfactants and PEGylated polymers can inhibit the activity of cytochrome P450[20,21]. PEG-PLA monomers can inhibit the activity of P-glycoprotein[22] and PEG 2000 has been shown to inhibit the activity of multidrug resistance-associated protein 2 (MRP2)[23]. Inhibition of such enzymes and transporters may lead to significant changes in exposure to certain drugs.

Concern has been expressed about the safety of PNMs and the side effects associated with their long-term use[24]. This is because PNMs can be recognized and engulfed by phagocytes of the reticuloendothelial system (RES) and remain in the liver and spleen for long periods of time. If the PNM cannot be biodegraded, it may accumulate in these organs leading to toxicity and side effects[25]. If it can be biodegraded, the degradation products may not be biocompatible[25]. Therefore, in the design and optimization of PNMs, it is important to establish not only their efficacy but also their biological fate. This requires an investigation of the biodistribution, metabolism and transport of PNMs at the tissue level which, in turn, requires a quantitative analytical method for the determination of PNMs in biofluids, tissues and organs[26]. This presents a major challenge because most polymers in PNMs are high molecular weight, polydisperse molecules.

In this paper, we report a study of the *in vivo* fate of PEG-PLA in rat using a liquid chromatography tandem mass spectrometric method developed in our laboratory for the quantitative analysis of PEG-PLA based on the MS^{ALL} technique. PEG-PLA is an amphiphilic di-block copolymer composed of PEG and PLA that is commonly used as a PNM. When the concentration of PEG-PLA in aqueous solution is higher than its critical micelle concentration (CMC), it self-assembles to form polymeric micelles. Polymeric micelles are core-shell structures that composed of shells of the hydrophilic block and cores of the hydrophobic block of the amphiphilic di-block copolymer. A paclitaxel formulation of PEG-PLA based polymeric micelle, known as Genexol-PM, has been approved by the FDA for the treatment of breast cancer[27,28]. The development of a suitable analytical technique for PEG-PLA and a full understanding of its *in vivo* fate will further promote the development of other nanoparticle (NP) chemotherapeutics.

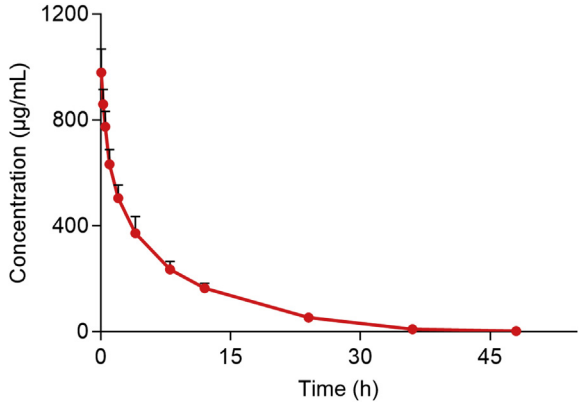

Figure 1 Mean plasma concentration-time curve of PEG-PLA after a single intravenous injection of 37.5 mg/kg PEG-PLA to rat (data are mean ± SD, $n = 6$).

2. Materials and methods

2.1. Chemicals and reagents

PEG-PLA (PEG average MW 2000 Da, PLA average MW 2000 Da) and *O*,*O*-dimethyl *O*-(2,2-dichlorovinyl) phosphate (DDVP) were purchased from Sigma–Aldrich (St. Louis, MO, USA). HPLC grade acetonitrile, isopropanol, water, ammonium acetate and formic acid were purchased from Fisher Chemical (Fair Lawn, NJ, USA).

2.2. Sample preparation

For plasma, tissue homogenate and urine, 450 μL acetonitrile was added to a 50 μL aliquot of sample in a 2 mL tube and shaken for 60 s. The sample was then centrifuged at 4 °C, 13,300 rpm for 5 min using a Heraeus Pico17 centrifuge (Thermo Scientific, Waltham, MA, USA), after which the supernatant (tissue homogenate and urine) was removed for analysis, or (plasma) 50 μL supernatant was mixed well with 450 μL acetonitrile:water (90:10, *v*/*v*) for analysis. Bile samples were processed in the same way as tissue homogenate and urine except 250 μL acetonitrile was added to a 50 μL aliquot of sample.

2.3. Liquid chromatography tandem mass spectrometry

Chromatography was performed on a SIL-20A XR HPLC system (Shimadzu, Kyoto, Japan) using gradient elution on an Agilent Poroshell 300SB C18 (75 mm × 2.1 mm, 5 μm) column. The mobile phase consisted of 0.1% formic acid and 5 mmol/L ammonium acetate in water (solvent A) and acetonitrile:isopropanol (50:50, *v*/*v*)

Table 1 Pharmacokinetic parameters of PEG-PLA in rat plasma after a single intravenous injection of 37.5 mg/kg PEG-PLA.

Parameter	Mean	SD
C_0 (μg/mL)	998	100
C_{max} (μg/mL)	979	90
T_{max} (h)	0.033	0.001
$t_{1/2}$ (h)	5.90	0.50
AUC_{0-t} (h·μg/mL)	5998	620
$AUC_{0-\infty}$ (h·μg/mL)	6020	620
CL (mL/h/kg)	6.28	0.65
V_z (mL/kg)	53.6	8.5

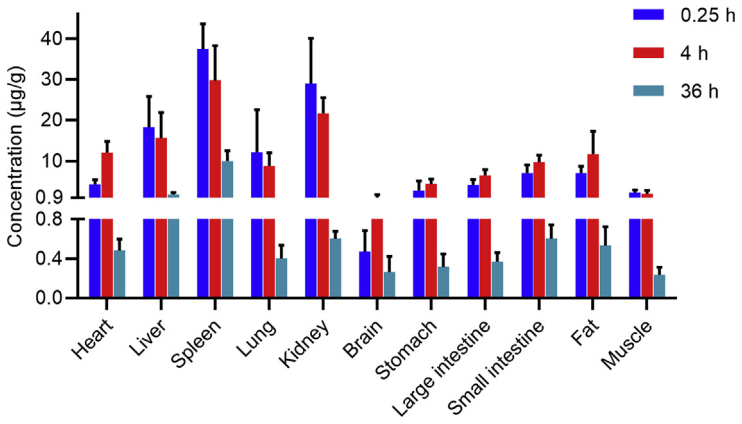

Figure 2 The biodistribution of PEG-PLA in rat at 0.25, 4 and 36 h after a single intravenous injection of 37.5 mg/kg PEG-PLA (data are mean ± SD, $n = 6$).

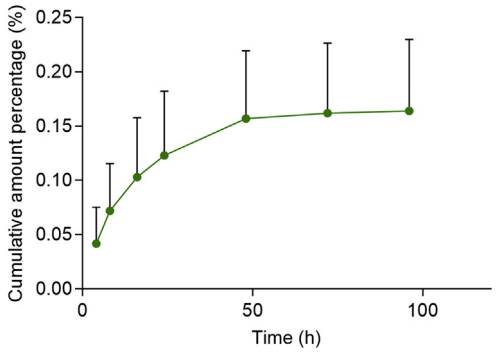

Figure 3 Mean cumulative excretion–time curve for PEG-PLA in rat bile after a single intravenous injection of 37.5 mg/kg PEG-PLA (data are mean ± SD, $n = 7$).

(solvent B) delivered at 0.3 mL/min according to the following gradient: 0–0.75 min 20% B, 1.3–4 min 90% B, 4.2–6.5 min 20% B.

Detection was carried out on a SCIEX Triple TOF 5600 mass spectrometer (AB SCIEX, Foster City, CA, USA) operated with positive electrospray ionization (ESI) using MS^{ALL} with a scan range of 100–1500 Da. ESI source parameters were set as follows: Spray voltage 5500 V; nebulizer gas 45 psi; heating gas 45 psi; curtain gas 25 psi; ion source temperature, 450 °C. Declustering potential (DP) was 50 V and collision energy (CE) was 35 eV.

Calibration curves were used for the quantification of PEG-PLA. Calibration curves were constructed based on the peak area and nominal concentration of PEG-PLA by linear least-squares regression with $1/x^2$ weighting. The method performance was evaluated and the results (shown in Supporting Information Figs. S1–S4 and Tables S1–S6) showed that the method could be used for the quantification of PEG-PLA in biological samples.

2.4. *Animal studies*

Sprague–Dawley rats (weight 200 ± 20 g) were obtained from the Animal Center of Yanbian University, China. All animal experiments were carried using equal numbers of males and females unless otherwise stated. Experiments were carried out in accordance with the Guiding Principles of the Jilin University Animal Ethics Committee.

2.4.1. *Pharmacokinetic study*

A group of 6 rats was administered single 37.5 mg/kg doses of PEG-PLA by tail vein injection of a 15 mg/mL solution in saline. Blood samples (200 μL) were collected before the dose and at 0.033, 0.25, 0.5, 1, 2, 4, 8, 12, 24, 36, and 48 h after the dose into heparinized tubes containing 0.05% DDVP. Plasma was obtained by centrifugation at 13,300 rpm for 5 min. Phoenix WinNonlin 6.4 software was used to calculate non-compartmental pharmacokinetic parameters.

2.4.2. *Biodistribution*

A group of 18 rats were randomly divided into three equal groups and administered single 37.5 mg/kg doses of PEG-PLA through the tail vein. Organs and tissues (heart, liver, spleen, lung, kidney, stomach, small intestine, large intestine, brain, fat and muscle) were harvested from groups of 6 rats (3 male, 3 female) at 0.25, 4, and 36 h after administration. Organs and tissues (0.5 g) were then homogenized in 2 mL acetonitrile-water (10:90, *v*/*v*) containing 0.05% DDVP by grinding for 30 s in a vibrating ball mill at 1200 rpm (Detailed instructions on the preparation of tissue homogenate are shown in Note S-1).

2.4.3. *Metabolism and excretion*

For the study of urine excretion, 6 rats were placed in individual metabolic cages for 12 h during which blank urine was collected. Each rat was then administered a single tail vein 37.5 mg/kg injection of PEG-PLA after which urine was collected over the time periods 0–4, 4–8, 8–12, 12–24, 24–48, 48–72 and 72–96 h and the volumes recorded.

For the study of biliary excretion, a group of 7 rats (3 males and 4 females) were anesthetized and subjected to bile cannulation. Single 37.5 mg/kg tail vein injections of PEG-PLA were then administered and bile collected during the time periods 0–4, 4–8, 8–16, 16–24, 24–48, 48–72, 72–96 and the volumes recorded.

3. Results and discussion

3.1. *Pharmacokinetics*

The average plasma concentration-time curve of PEG-PLA after a single 37.5 mg/kg intravenous injection is shown in Fig. 1 with corresponding pharmacokinetic parameters given in Table 1 (the detailed data of each rat is shown in Supporting Information

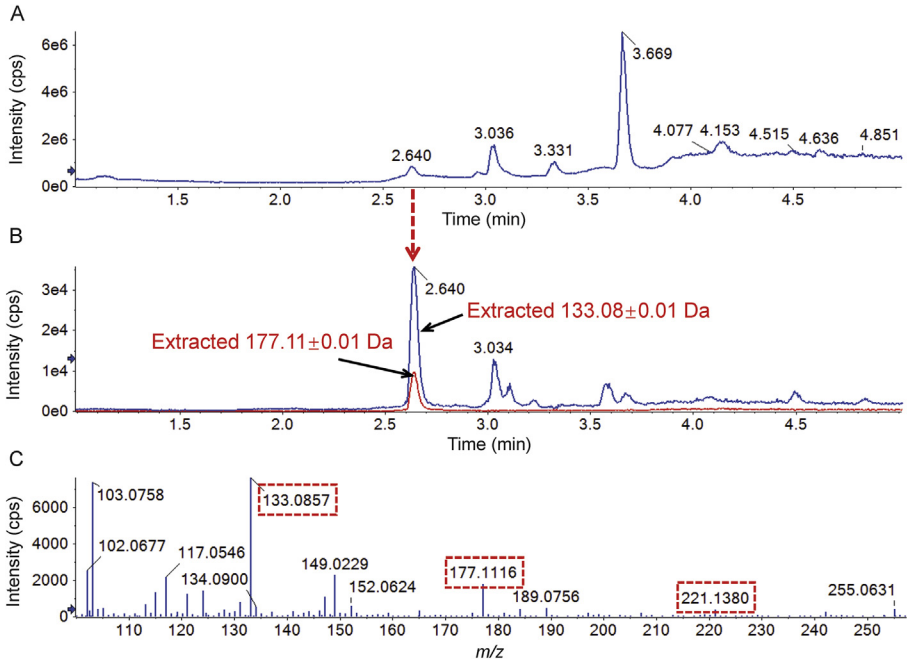

Figure 4 Application of the MS^{ALL} technique to the detection of PEG produced by metabolism of PEG-PLA in rat urine. (A) Total ion chromatogram; (B) extracted ion chromatograms of PEG showing PEG characteristic fragment ions at *m/z* 133.08 and 177.11; and (C) the mass spectrum of PEG.

Table S6). The elimination half-life ($t_{1/2}$) of 5.90 ± 0.50 h indicates PEG-PLA is eliminated slowly in rat. The apparent volume of distribution (V_z) of 53.6 ± 8.5 mL/kg is greater than the volume of rat plasma (31.2 mL/kg) but less than the volume of rat extracellular fluid (296.8 mL/kg)[29], indicating PEG-PLA is mainly distributed in plasma and extracellular fluid. The area under the concentration-time curve (AUC_{0-t}) of 6000 ± 620 h·μg/mL accounts for >99% of the $AUC_{0-\infty}$ of 6020 ± 619 h·μg/mL indicating that PEG-PLA is eliminated almost completely in rat plasma after 48 h.

3.2. *Biodistribution*

The distribution of a compound to tissues is affected by blood flow, permeability, tissue perfusion rate, affinity for plasma proteins and tissues, and physiological barriers (such as the blood–

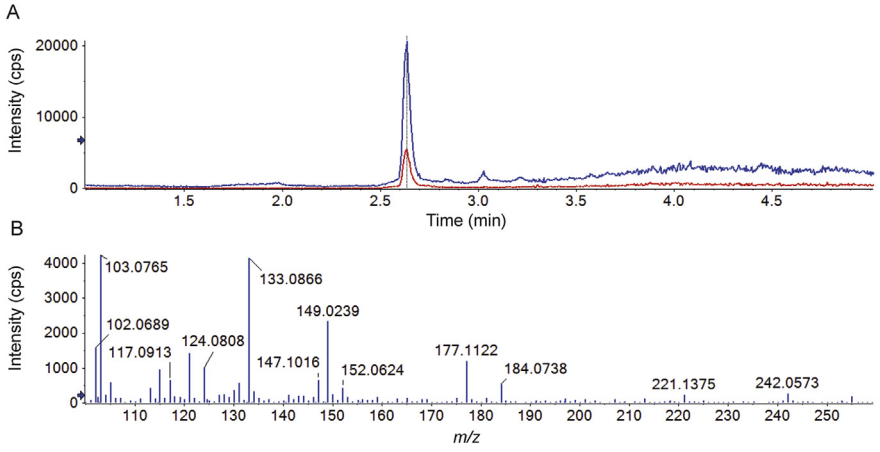

Figure 5 (A) Chromatogram of a blank rat urine sample spiked with PEG 2000 at 50 μg/mL showing extracted fragment ions at 133.08 ± 0.01 Da (blue) and 177.11 ± 0.01 Da (red) and (B) the mass spectrum of PEG 2000.

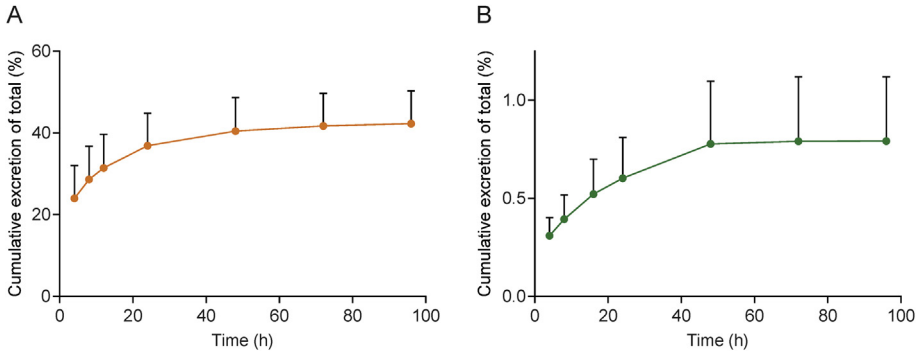

Figure 6 Mean cumulative excretion–time curves of PEG in (A) rat urine ($n = 6$) and (B) bile ($n = 7$) after a single intravenous injection of 37.5 mg/kg PEG-PLA (data are mean ± SD).

brain barrier). Initially, a polymer distributes into the intracellular and intercellular fluids through the circulatory system. PNM then distributes rapidly to organs with high perfusion rate such as the liver, kidneys and heart and has only limited distribution to tissues with low perfusion rate such as muscle and fat[2]. Many studies have pointed out that the distribution of PNM to the liver and spleen is higher than to other tissues[30,31] due to the high activity of the RES in these organs. In fact, RES clearance has been shown to be the main route of elimination of PNMs from the body[32].

The biodistribution of PEG-PLA to different tissues is shown in Fig. 2. As expected, the concentrations of PEG-PLA in spleen, liver, and kidney are relatively high while that in muscle is relatively low. The concentration is also relatively low in brain presumably because of the poor permeability of PEG-PLA through the blood–brain barrier. Surprisingly, the concentration of PEG-PLA in heart is also relatively low despite the fact that the heart is also a high perfusion rate organ. Possibly this is due to the low activity of the RES in the heart. In contrast the concentration of PEG-PLA in fat is relatively high presumably due to the high lipophilicity of the PLA component of PEG-PLA.

3.3. *Metabolism and excretion*

PEG-PLA was undetectable in urine indicating it is not cleared by renal excretion. Excretion into bile (Fig. 3) was also very low at <0.2% of the administered dose. These results indicate that, although limited in extent, PEG-PLA is mainly excreted into bile. This is consistent with the fact that in aqueous solution PEG-PLA undergoes self-assembly to form nanoscale micelles that are inflexible and too big (particle size >20 nm) to undergo glomerular filtration (size limit 10 nm)[33]. The fact that PEG-PLA micelles are in equilibrium with free PEG-PLA then raises the question of why free PEG-PLA is unable to undergo renal clearance. Presumably this is because of the lipophilicity of the PLA component of amphiphilic PEG-PLA.

Considering that the PLA in PEG-PLA is biodegradable[34–37], it is reasonable to expect that PEG-PLA would be metabolized to form PEG. Given that the MS^{ALL} technique can simultaneously acquire fragment ion information generated by all precursor ions[35,38,39], the presence of PEG can be shown by extracting PEG characteristic fragment ions from the acquired MS^{ALL} data. In this experiment, two PEG characteristic fragment ions at *m*/*z* 133.08 and 177.11 were extracted from the total ion chromatogram (Fig. 4) indicating that PEG-PLA is indeed metabolized to PEG.

The average MW of PEG in PEG-PLA used in this experiment was 2000 Da. The chromatogram and mass spectrum of PEG extracted in Fig. 4 are compared with those of a PEG 2000 standard (Fig. 5). The results show that the retention time (Fig. 4B) and mass spectrum (Fig. 4C) of the PEG extracted from the rat urine sample are similar to those of the PEG 2000 standard (Fig. 5) providing further evidence for the formation of PEG by PEG-PLA metabolism.

In addition, we determined the amount of PEG in rat urine and bile samples using our previously published method[40]. The cumulative amount of PEG excreted into urine accounted for more than 40% of the dose of PEG-PLA (Fig. 6A) while that in bile accounted for <0.8% of the dose (Fig. 6B). This indicates that the PEG produced by PEG-PLA metabolism is mainly excreted through the kidney. The total amount of PEG excreted in urine and bile accounted for 43% of the PEG-PLA dose.

Since the amount of PEG excreted accounts for about 50% of the mass fraction of PEG-PLA, the cumulative amount of PEG-PLA excreted can be calculated to be approximately 86%. Thus, it can be concluded that PEG-PLA administered by intravenus injection is mainly excreted in urine as PEG.

4. Conclusions

The results of this study provide a comprehensive description of the biological fate of PEG-PLA in rat. They show that PEG-PLA is almost completely eliminated from rat plasma over a period of 48 h although only small amounts of intact PEG-PLA are excreted most being metabolized to PEG and subsequently eliminated in urine. High concentrations of PEG-PLA are found in organs with high perfusion rate and a highly active RES. We anticipate our findings will facilitate the design and safety evaluation of PEG-PLA-based nanocarrier drug delivery systems and promote their clinical development.

Acknowledgments

This work was supported by the National Natural Science Foundation of China (Grant Nos. 81872831 and 82030107) and the National Science and Technology Major Projects for significant new drugs creation of the 13th five-year plan (2017ZX09101001 and 2018ZX09721002007, China).

Author contributions

Xiangjun Meng and Jingkai Gu designed the research. Xiangjun Meng, Zhi Zhang, Jin Tong and Hui Sun carried out the experiments and performed data analysis. Xiangjun Meng, John Paul Fawcett and Jingkai Gu wrote the manuscript. All of the authors have read and approved the final manuscript.

Conflicts of interest

The authors have no conflicts of interest to declare.

Appendix A. Supporting information

Supporting data to this article can be found online at https://doi.org/10.1016/j.apsb.2021.02.018.

References

1. Su H, Wang Y, Liu S, Wang Y, Liu Q, Liu G, et al. Emerging transporter-targeted nanoparticulate drug delivery systems. *Acta Pharm Sin B* 2019;**9**:49−58.
2. Zhao QH, Qiu LY. An overview of the pharmacokinetics of polymer-based nanoassemblies and nanoparticles. *Curr Drug Metab* 2013;**14**:832−9.
3. Wang AZ, Langer R, Farokhzad OC. Nanoparticle delivery of cancer drugs. *Annu Rev Med* 2012;**63**:185−98.
4. Liu GW, Prossnitz AN, Eng DG, Cheng Y, Subrahmanyam N, Pippin JW, et al. Glomerular disease augments kidney accumulation of synthetic anionic polymers. *Biomaterials* 2018;**178**:317−25.
5. Li J, Burgess DJ. Nanomedicine-based drug delivery towards tumor biological and immunological microenvironment. *Acta Pharm Sin B* 2020;**10**:2110−24.
6. Buggins TR, Dickinson PA, Taylor G. The effects of pharmaceutical excipients on drug disposition. *Adv Drug Deliv Rev* 2007;**59**:1482−503.
7. Goole J, Lindley DJ, Roth W, Carl SM, Amighi K, Kauffmann JM, et al. The effects of excipients on transporter mediated absorption. *Int J Pharm* 2010;**393**:17−31.
8. Cornaire G, Woodley J, Hermann P, Cloarec A, Arellano C, Houin G. Impact of excipients on the absorption of P-glycoprotein substrates *in vitro* and *in vivo*. *Int J Pharm* 2004;**278**:119−31.
9. Ren X, Mao X, Si L, Cao L, Xiong H, Qiu J, et al. Pharmaceutical excipients inhibit cytochrome P450 activity in cell free systems and after systemic administration. *Eur J Pharm Biopharm* 2008;**70**:279−88.
10. Huang WX, Desai M, Tang Q, Yang R, Vivilecchia RV, Joshi Y. Elimination of metformin-croscarmellose sodium interaction by competition. *Int J Pharm* 2006;**311**:33−9.
11. Rafiei P, Haddadi A. Docetaxel-loaded PLGA and PLGA-PEG nanoparticles for intravenous application: pharmacokinetics and biodistribution profile. *Int J Nanomedicine* 2017;**12**:935−47.
12. Wang Q, Liu Y, Pu C, Zhang H, Tan X, Gou J, et al. Drug-polymer interaction, pharmacokinetics and antitumor effect of PEG-PLA/taxane derivative TM-2 micelles for intravenous drug delivery. *Pharm Res* 2018;**35**:208.
13. Balachandra A, Chan EC, Paul JP, Ng S, Chrysostomou V, Ngo S, et al. A biocompatible reverse thermoresponsive polymer for ocular drug delivery. *Drug Deliv* 2019;**26**:343−53.
14. Singh P, Carrier A, Chen Y, Lin S, Wang J, Cui S, et al. Polymeric microneedles for controlled transdermal drug delivery. *J Control Release* 2019;**315**:97−113.
15. Rajput MKS, Kesharwani SS, Kumar S, Muley P, Narisetty S, Tummala H. Dendritic cell-targeted nanovaccine delivery system prepared with an immune-active polymer. *ACS Appl Mater Interfaces* 2018;**10**:27589−602.
16. Battistella C, Klok HA. Controlling and monitoring intracellular delivery of anticancer polymer nanomedicines. *Macromol Biosci* 2017;**17**.
17. Dou T, Wang J, Han C, Shao X, Zhang J, Lu W. Cellular uptake and transport characteristics of chitosan modified nanoparticles in Caco-2 cell monolayers. *Int J Biol Macromol* 2019;**138**:791−9.
18. Wang T, Guo Y, He Y, Ren T, Yin L, Fawcett JP, et al. Impact of molecular weight on the mechanism of cellular uptake of polyethylene glycols (PEGs) with particular reference to P-glycoprotein. *Acta Pharm Sin B* 2020;**10**:2002−9.
19. Kermanizadeh A, Balharry D, Wallin H, Loft S, Møller P. Nanomaterial translocation—the biokinetics, tissue accumulation, toxicity and fate of materials in secondary organs—a review. *Crit Rev Toxicol* 2015;**45**:837−72.
20. Martin P, Giardiello M, McDonald TO, Rannard SP, Owen A. Mediation of *in vitro* cytochrome p450 activity by common pharmaceutical excipients. *Mol Pharm* 2013;**10**:2739−48.
21. Qiu L, Li Q, Huang J, Wu Q, Tu K, Wu Y, et al. *In vitro* effect of mPEG(2k)-PCL(x) micelles on rat liver cytochrome P450 enzymes. *Int J Pharm* 2018;**552**:99−110.
22. Li W, Li X, Gao Y, Zhou Y, Ma S, Zhao Y, et al. Inhibition mechanism of P-glycoprotein mediated efflux by mPEG-PLA and influence of PLA chain length on P-glycoprotein inhibition activity. *Mol Pharm* 2014;**11**:71−80.
23. Li L, Yi T, Lam CW. Interactions between human multidrug resistance related protein (MRP2; ABCC2) and excipients commonly used in self-emulsifying drug delivery systems (SEDDS). *Int J Pharm* 2013;**447**:192−8.
24. Stevanović M, Maksin T, Petković J, Filipic M, Uskoković D. An innovative, quick and convenient labeling method for the investigation of pharmacological behavior and the metabolism of poly(D,L-lactide-co-glycolide) nanospheres. *Nanotechnology* 2009;**20**:335102.
25. Peracchia MT, Fattal E, Desmaële D, Besnard M, Noël JP, Gomis JM, et al. Stealth PEGylated polycyanoacrylate nanoparticles for intravenous administration and splenic targeting. *J Control Release* 1999;**60**:121−8.
26. Drasler B, Vanhecke D, Rodriguez-Lorenzo L, Petri-Fink A, Rothen-Rutishauser B. Quantifying nanoparticle cellular uptake: which method is best?. *Nanomedicine (Lond)* 2017;**12**:1095−9.
27. Oerlemans C, Bult W, Bos M, Storm G, Nijsen JF, Hennink WE. Polymeric micelles in anticancer therapy: targeting, imaging and triggered release. *Pharm Res* 2010;**27**:2569−89.
28. Kore G, Kolate A, Nej A, Misra A. Polymeric micelle as multifunctional pharmaceutical carriers. *J Nanosci Nanotechnol* 2014;**14**:288−307.
29. Davies B, Morris T. Physiological parameters in laboratory animals and humans. *Pharm Res* 1993;**10**:1093−5.
30. Fraser JR, Laurent TC, Pertoft H, Baxter E. Plasma clearance, tissue distribution and metabolism of hyaluronic acid injected intravenously in the rabbit. *Biochem J* 1981;**200**:415−24.
31. Wood KM, Wusteman FS, Curtis CG. The degradation of intravenously injected chondroitin 4-sulphate in the rat. *Biochem J* 1973;**134**:1009−13.
32. Moghimi SM, Hunter AC. Capture of stealth nanoparticles by the body's defences. *Crit Rev Ther Drug Carrier Syst* 2001;**18**:527−50.
33. Popielarski SR, Hu-Lieskovan S, French SW, Triche TJ, Davis ME. A nanoparticle-based model delivery system to guide the rational design of gene delivery to the liver. 2. *In vitro* and *in vivo* uptake results. *Bioconjug Chem* 2005;**16**:1071−80.
34. Tsuji H, Ikarashi K. *In vitro* hydrolysis of poly(L-lactide) crystalline residues as extended-chain crystallites. Part I: long-term hydrolysis in phosphate-buffered solution at 37 degrees C. *Biomaterials* 2004;**25**:5449−55.

35. Gillet LC, Navarro P, Tate S, Röst H, Selevsek N, Reiter L, et al. Targeted data extraction of the MS/MS spectra generated by data-independent acquisition: a new concept for consistent and accurate proteome analysis. *Mol Cell Proteomics* 2012;**11**. O111.016717.
36. Letchford K, Burt H. A review of the formation and classification of amphiphilic block copolymer nanoparticulate structures: micelles, nanospheres, nanocapsules and polymersomes. *Eur J Pharm Biopharm* 2007;**65**:259−69.
37. Sharma D, Singh J. Long-term glycemic control and prevention of diabetes complications *in vivo* using oleic acid-grafted-chitosan-zinc-insulin complexes incorporated in thermosensitive copolymer. *J Control Release* 2020;**323**:161−78.
38. Zhu X, Chen Y, Subramanian R. Comparison of information-dependent acquisition, SWATH, and MS(All) techniques in metabolite identification study employing ultrahigh-performance liquid chromatography-quadrupole time-of-flight mass spectrometry. *Anal Chem* 2014;**86**:1202−9.
39. Gao F, McDaniel J, Chen EY, Rockwell HE, Nguyen C, Lynes MD, et al. Adapted MS/MS(ALL) shotgun lipidomics approach for analysis of cardiolipin molecular species. *Lipids* 2018;**53**:133−42.
40. Zhou X, Meng X, Cheng L, Su C, Sun Y, Sun L, et al. Development and application of an MS(ALL)-based approach for the quantitative analysis of linear polyethylene glycols in rat plasma by liquid chromatography triple-quadrupole/time-of-flight mass spectrometry. *Anal Chem* 2017;**89**:5193−200.